INTERNATIONAL JOURNAL FOR NUMERICAL AND ANALYTICAL METHODS IN GEOMECHANICS
Int. J. Numer. Anal. Meth. Geomech., 2001; **25**:307–327

Finite element analysis of land subsidence above depleted reservoirs with pore pressure gradient and total stress formulations

Giuseppe Gambolati[1,*,†], Massimiliano Ferronato[1], Pietro Teatini[1], Roberto Deidda[2] and Giuditta Lecca[2]

[1]*DMMMSA - Department of Mathematical Methods and Models for Scientific Applications, University of Padova, Via Belzoni 7, 35131 Padova, Italy*
[2]*CRS4 - Centro di Ricerca, Sviluppo e Studi Superiori in Sardegna VI Strada Ovest, Z.I. Macchiareddu, 09010 Cagliari, Italy*

SUMMARY

The solution of the poroelastic equations for predicting land subsidence above productive gas/oil fields may be addressed by the principle of virtual works using either the effective intergranular stress, with the pore pressure gradient regarded as a distributed body force, or the total stress incorporating the pore pressure. In the finite element (FE) method both approaches prove equivalent at the global assembled level. However, at the element level apparently the equivalence does not hold, and the strength source related to the pore pressure seems to generate different local forces on the element nodes. The two formulations are briefly reviewed and discussed for triangular and tetrahedral finite elements. They are shown to yield different results at the global level as well in a three-dimensional axisymmetric porous medium if the FE integration is performed using the average element-wise radius. A modification to both formulations is suggested which allows to correctly solve the problem of a finite reservoir with an infinite pressure gradient, i.e. with a pore pressure discontinuity on its boundary. Copyright © 2001 John Wiley & Sons, Ltd.

KEY WORDS: finite elements; land subsidence; pore pressure gradient; total stress; average element-wise radius; infinite pressure gradient

1. INTRODUCTION

Poroelastic theory is the basis for the simulation and prediction of land subsidence above productive gas/oil fields [1]. This problem may be addressed by two different approaches, i.e. the uncoupled (e.g. Reference [2]) or the coupled modelling (e.g. Reference [3]). In the latter case the

* Correspondence to: G. Gambolati, DMMMSA—Department of Mathematical Methods and Models for Scientific Applications, University of Padova, Via Belzoni 7, 35131 Padova, Italy
† E-mail: gambo@dmsa.unipd.it

Contract/grant sponsor: Italian MURST Project
Contract/grant sponsor: Sardinian Regional Authorities

Received 29 November 1999
Revised 25 August 2000

poroelastic and fluid dynamic equations are solved together for the pore pressure and medium displacement unknowns. Following the former approach instead, after the fluid pressure distribution within (and around) a reservoir is independently obtained with either a flow simulator or *in situ* measurements, the settlement of land surface is provided by a poroelastic model only. Typically, finite elements (FE) are used to discretize the porous medium [4,5]. In both approaches the discrete poroelastic equilibrium equations can be derived using a 'total stress' or a 'pressure gradient' formulation [6], in the latter case the pore pressure gradient being regarded as an external source of strength, i.e. a distributed (known or unknown) body force per unit volume. Both formulations have been followed in the literature. The pressure gradient formulation is used by [7–10] and [11], while the total stress formulation is used by [3,12], and [13].

For the arguments and derivations that follow it is irrelevant to think of the pore pressure as being known or unknown. Since coupling requires a much higher computational burden, with a possible ill-conditioning of the resulting discretized equations (e.g. References [14–16]), for the sake of simplicity the analysis that follows is performed in an uncoupled (isotropic) context. The findings turn out to be fully general and can be readily extended to a coupled (anisotropic) formulation as well.

At the global assembled level the pressure gradient and total stress approaches are fully equivalent. However, at the element level they are not, if as usual inter-element boundary integrals are ignored, and produce a different expression for the local loads applied on the element nodes. The standard FE implementation does not introduce any error into the final model since assembling cancels the contributions arising from the integrals extended to the internal element boundaries. Since the formal equivalence is not being sought when the FE integration is performed over each single element, the different expressions taken on by the local nodal forces should not be surprising. Moreover, for the three-dimensional axisymmetric model making use of the average element-wise radius, the formulations do not numerically coincide at the global level as well, and yield a different prediction of land subsidence in the vicinity of the symmetry axis.

In the present paper we address the issue of the equivalence of the pore pressure gradient and total stress approaches for the FE integration of the poroelastic equations in a porous medium embedding a depleted gas/oil reservoir. First, both formulations are briefly reviewed and shown to be equivalent when appropriate boundary integrals are accounted for. Next, the local nodal forces are derived in two- and three-dimensional settings for triangular, tetrahedral and annular elements with a triangular cross-section. An argument is given to explain the different results from the two formulations when used in three-dimensional axisymmetric models with average element-wise radii. The influence of a pumping well with a finite radius giving rise to a boundary integral on the well wall in the total stress approach is discussed. Finally, the problem with an infinite pressure gradient, i.e. a reservoir where the pore pressure exhibits a discontinuity on its boundary, is solved exactly in both formulations properly modified.

2. REVIEW OF BASIC THEORY

Let us assume an orthogonal three dimensional x, y, z reference frame. We use a vector and matrix notation with bold lower case for vectors and italic upper case for matrices. Start from an initial equilibrium configuration and express all the variables related to stress, strain, and displacement in terms of incremental quantities. If $\hat{\boldsymbol{\sigma}}^{\mathrm{T}} = [\hat{\sigma}_x, \hat{\sigma}_y, \hat{\sigma}_z, \hat{\sigma}_{xy}, \hat{\sigma}_{yz}, \hat{\sigma}_{xz}]$ and p denote the vector of the total stress components and the pore pressure, respectively, at any point of the

poroelastic medium, Terzaghi's effective stress principle reads [17, 6]:

$$\hat{\boldsymbol{\sigma}} = \boldsymbol{\sigma} - \mathbf{i}p \tag{1}$$

where $\boldsymbol{\sigma}^{\mathrm{T}} = [\sigma_x, \sigma_y, \sigma_z, \sigma_{xy}, \sigma_{yz}, \sigma_{xz}]$ indicates the vector of effective (grain to grain) stresses and $\mathbf{i}^{\mathrm{T}} = [1, 1, 1, 0, 0, 0]$ represents the Kronecker δ in vectorial form. If $\hat{\mathbf{t}}$ and $\mathbf{t}$ denote the total and effective force per unit surface, respectively, and $\mathbf{n}$ the outer normal to the boundary of the porous medium we have

$$\hat{\mathbf{t}} = \mathbf{t} - \mathbf{n}p \tag{2}$$

In the above equations we adopt the sign convention that tensile stresses and pore pressures are positive.

The deformation of the porous body is described by the strain component vector $\boldsymbol{\varepsilon}$ and the displacement vector $\mathbf{u}$.

The equilibrium equations for the porous medium including both the solid grains and the fluid are

$$\begin{aligned} \frac{\partial \hat{\sigma}_x}{\partial x} + \frac{\partial \hat{\sigma}_{xy}}{\partial y} + \frac{\partial \hat{\sigma}_{xz}}{\partial z} &= 0 \\ \frac{\partial \hat{\sigma}_{xy}}{\partial x} + \frac{\partial \hat{\sigma}_y}{\partial y} + \frac{\partial \hat{\sigma}_{yz}}{\partial z} &= 0 \\ \frac{\partial \hat{\sigma}_{xz}}{\partial x} + \frac{\partial \hat{\sigma}_{yz}}{\partial y} + \frac{\partial \hat{\sigma}_z}{\partial z} &= 0 \end{aligned} \tag{3}$$

Replacing Equation (1) into Equations (3) yields

$$\begin{aligned} \frac{\partial \sigma_x}{\partial x} + \frac{\partial \sigma_{xy}}{\partial y} + \frac{\partial \sigma_{xz}}{\partial z} - \frac{\partial p}{\partial x} &= 0 \\ \frac{\partial \sigma_{xy}}{\partial x} + \frac{\partial \sigma_y}{\partial y} + \frac{\partial \sigma_{yz}}{\partial z} - \frac{\partial p}{\partial y} &= 0 \\ \frac{\partial \sigma_{xz}}{\partial x} + \frac{\partial \sigma_{yz}}{\partial y} + \frac{\partial \sigma_z}{\partial z} - \frac{\partial p}{\partial z} &= 0 \end{aligned} \tag{4}$$

2.1. Pore pressure gradient formulation

In Equations (4) the pore pressure gradient can be regarded as a distributed force for unit volume $\mathbf{q}$:

$$\mathbf{q} = -\operatorname{grad}(p) = -\nabla p$$

Let us state the virtual work principle for the whole porous medium. The internal virtual work is done by the effective stress components while the external work is performed by the effective stress acting on the boundary Σ plus the pore pressure gradient acting on the porous volume V:

$$\int_V \boldsymbol{\varepsilon}^{\mathrm{T}} \boldsymbol{\sigma} \, \mathrm{d}V = \int_V \mathbf{u}^{\mathrm{T}} \mathbf{q} \, \mathrm{d}V + \int_\Sigma \mathbf{u}^{\mathrm{T}} \mathbf{t} \, \mathrm{d}\Sigma \tag{5}$$

2.2. Total stress formulation

The virtual work principle applies to the system made of the porous matrix plus the fluid with the work done by the total stress and the total forces per unit surface on the boundary. It can be written as

$$\int_V \boldsymbol{\varepsilon}^{\mathrm{T}} \hat{\boldsymbol{\sigma}} \, \mathrm{d}V = \int_\Sigma \mathbf{u}^{\mathrm{T}} \hat{\mathbf{t}} \, \mathrm{d}\Sigma \tag{6}$$

Using Equations (1) and (2), Equation (6) becomes

$$\int_V \boldsymbol{\varepsilon}^{\mathrm{T}} \boldsymbol{\sigma} \, \mathrm{d}V = \int_V \boldsymbol{\varepsilon}^{\mathrm{T}} \mathbf{i} p \, \mathrm{d}V + \int_\Sigma \mathbf{u}^{\mathrm{T}} \mathbf{t} \, \mathrm{d}\Sigma - \int_\Sigma \mathbf{u}^{\mathrm{T}} \mathbf{n} p \, \mathrm{d}\Sigma \tag{7}$$

2.3. Equivalence of formulations

In Equation (7) the term $\boldsymbol{\varepsilon}^{\mathrm{T}}\mathbf{i}$ is the volume strain or dilatation, i.e. the divergence of the position vector $\mathbf{u}$: $\boldsymbol{\varepsilon}^{\mathrm{T}}\mathbf{i} = \mathrm{div}(\mathbf{u})$. Using Green's first identity yields

$$\int_V \boldsymbol{\varepsilon}^{\mathrm{T}} \mathbf{i} p \, \mathrm{d}V = \int_V \mathrm{div}(\mathbf{u}) p \, \mathrm{d}V = -\int_V \mathbf{u}^{\mathrm{T}} \nabla p \, \mathrm{d}V + \int_\Sigma \mathbf{u}^{\mathrm{T}} \mathbf{n} p \, \mathrm{d}\Sigma$$

Replacing the above result in Equation (7) leads to

$$\int_V \boldsymbol{\varepsilon}^{\mathrm{T}} \boldsymbol{\sigma} \, \mathrm{d}V = -\int_V \mathbf{u}^{\mathrm{T}} \nabla p \, \mathrm{d}V + \int_\Sigma \mathbf{u}^{\mathrm{T}} \mathbf{t} \, \mathrm{d}\Sigma = \int_V \mathbf{u}^{\mathrm{T}} \mathbf{q} \, \mathrm{d}V + \int_\Sigma \mathbf{u}^{\mathrm{T}} \mathbf{t} \, \mathrm{d}\Sigma$$

which is Equation (5). Hence the two formulations (5) and (7) are theoretically equivalent. The difference between the volume integrals on the right-hand side is compensated for in Equation (7) by the extra boundary integral $-\int_\Sigma \mathbf{u}^{\mathrm{T}} \mathbf{n} p \, \mathrm{d}\Sigma$.

3. FE SOLUTION TO THE POROELASTIC EQUATIONS

Equations (5) and (7) may be solved in real poroelastic media by the FE method [4,5]. In the sequel, the contributions arising from any single element are denoted by subscript e. The porous body is discretized into a number of elements and the local displacement $\mathbf{u}_e$ and pore pressure p_e are expressed as

$$\mathbf{u}_e = N \boldsymbol{\delta}_e$$

$$p_e = N_1 \mathbf{p}_e$$

where N and N_1 are shape (or basis) function matrices while $\boldsymbol{\delta}_e$ and $\mathbf{p}_e$ are local vectors containing the components of the nodal displacements and nodal pore pressure, respectively. The effective

stress vector $\boldsymbol{\sigma}_e$ is related to the strain vector $\boldsymbol{\varepsilon}_e$ through the elastic matrix D:

$$\boldsymbol{\sigma}_e = D\boldsymbol{\varepsilon}_e$$

The strain components $\boldsymbol{\varepsilon}_e$ are given by

$$\boldsymbol{\varepsilon}_e = L\mathbf{u}_e = LN\boldsymbol{\delta}_e = B\boldsymbol{\delta}_e$$

with L a first-order differential operator and $B = LN$ the strain matrix. Replacing the previous quantities into Equations (5) and (7) yields the local contributions to the FE solution to the poroelastic equations:

(1) *Pore pressure gradient formulation*:

$$\left(\int_{V_e} B^{\mathrm{T}} DB \,\mathrm{d}V\right)\boldsymbol{\delta}_e = \left(-\int_{V_e} N^{\mathrm{T}} \nabla N_1 \,\mathrm{d}V\right)\mathbf{p}_e + \int_{\Sigma_e} N^{\mathrm{T}}\mathbf{t}_e \,\mathrm{d}\Sigma$$

namely

$$K_e\boldsymbol{\delta}_e = Q_{g,e}\mathbf{p}_e + \tilde{\mathbf{f}}_{t,e} \tag{8}$$

where K_e is the local elastic stiffness matrix, $Q_{g,e}$ is the local matrix which relates the displacement to the unknown pore pressure in the coupled approach, hence it will be called the coupling matrix, and $\tilde{\mathbf{f}}_{t,e}$ is the vector of the local effective forces.

(2) *Total stress formulation*:

$$\left(\int_{V_e} B^{\mathrm{T}} DB \,\mathrm{d}V\right)\boldsymbol{\delta}_e = \left(\int_{V_e} B^{\mathrm{T}}\mathbf{i} N_1 \,\mathrm{d}V\right)\mathbf{p}_e + \int_{\Sigma_e} N^{\mathrm{T}}\mathbf{t}_e \,\mathrm{d}\Sigma + \left(-\int_{\Sigma_e} N^{\mathrm{T}}\mathbf{n} N_1 \,\mathrm{d}\Sigma\right)\mathbf{p}_e$$

namely

$$K_e\boldsymbol{\delta}_e = Q_{t,e}\,\mathbf{p}_e + \tilde{\mathbf{f}}_{t,e} + \tilde{\mathbf{f}}_{p,e} \tag{9}$$

where $Q_{t,e}$ may be regarded as another coupling matrix since the vector of the local forced $\tilde{\mathbf{f}}_{p,e}$ related to the pore pressure $\mathbf{p}_e$ is usually ignored.

Consider any internal surface $\Sigma_{e,i}$ shared by two adjacent elements. In Equations (8) and (9) the contributions to $\tilde{\mathbf{f}}_{t,e}$ and $\tilde{\mathbf{f}}_{p,e}$ from the integrals performed over $\Sigma_{e,i}$ when belonging to either element are equal and opposite in sign, and hence cancel. Therefore, for any internal node necessarily $Q_g\mathbf{p} = Q_t\mathbf{p}$ where Q_g and Q_t are the global assembled coupling matrices arising from the pore pressure gradient and the total stress formulations, respectively, and $\mathbf{p}$ is the global vector of the nodal pore pressure. Only for nodes lying on the porous medium boundary we may have $Q_g\mathbf{p} \neq Q_t\mathbf{p}$, the difference between these equations being accounted for by the components of $\tilde{\mathbf{f}}_p$ in Equation (9) which may be non zero on a boundary node.

When dealing with prediction of land subsidence due to gas/oil withdrawal, the porous medium is usually represented by a half-space with no external loads prescribed on the upper horizontal surface that bounds the semi-infinite medium. Hence, the following boundary conditions apply:

(a) $\mathbf{u} = 0$, $\mathbf{t} = 0$, and $p = 0$ for x, y, z approaching infinity;
(b) $\mathbf{t} = 0$ and $p = 0$ at $z = 0$;

with the origin of the positive downward vertical z-axis set on a point of the boundary plane. For this problem $\tilde{\mathbf{f}}_p$ and $\tilde{\mathbf{f}}_t$ on the boundary nodes vanish and hence $Q_g = Q_t$ despite the fact that the local matrices $Q_{g,e}$ and $Q_{t,e}$ are different.

In the next sections matrices $Q_{g,e}$ and $Q_{t,e}$ are derived in two, three, and three-dimensional axisymmetric porous structures using triangular, tetrahedral and annular elements with a triangular cross-section.

3.1. Triangular elements

If i, j, and m are the numbers which define the triangle nodes listed in an anti-clockwise sense, the basis function N_i reads

$$N_i = \frac{a_i + b_i x + c_i y}{2\Delta_e}$$

where:

$$a_i = x_j y_m - x_m y_j$$

$$b_i = y_j - y_m$$

$$c_i = x_m - x_j$$

$$\Delta_e = \text{triangle area}$$

N_j and N_m are obtained from N_i by a proper index permutation. The local coupling matrices defined in Equations (8) and (9) are

$$Q_{g,e} = -\int_{\Delta_e} N^{\mathrm{T}} \nabla N_1 \, \mathrm{d}\Delta = -\frac{1}{6}\begin{bmatrix} b_i & b_j & b_m \\ c_i & c_j & c_m \\ b_i & b_j & b_m \\ c_i & c_j & c_m \\ b_i & b_j & b_m \\ c_i & c_j & c_m \end{bmatrix}$$

$$Q_{t,e} = \int_{\Delta_e} B^{\mathrm{T}} \mathbf{i} N_1 \, \mathrm{d}\Delta = \frac{1}{6}\begin{bmatrix} b_i & b_i & b_i \\ c_i & c_i & c_i \\ b_j & b_j & b_j \\ c_j & c_j & c_j \\ b_m & b_m & b_m \\ c_m & c_m & c_m \end{bmatrix}$$

It could be proven that the global Q_g and Q_t rows corresponding to any internal node are equal.

3.2. Tetrahedral elements

If i, j, m, and p denote the nodes of a tetrahedron, the basis function N_i now reads

$$N_i = \frac{a_i + b_i x + c_i y + d_i z}{6V_e}$$

with a_i, b_i, c_i, d_i, and V_e given by

$$a_i = \begin{vmatrix} x_j & y_j & z_j \\ x_m & y_m & z_m \\ x_p & y_p & z_p \end{vmatrix}, \qquad b_i = -\begin{vmatrix} 1 & y_j & z_j \\ 1 & y_m & z_m \\ 1 & y_p & z_p \end{vmatrix}$$

$$c_i = \begin{vmatrix} 1 & x_j & z_j \\ 1 & x_m & z_m \\ 1 & x_p & z_p \end{vmatrix}, \qquad d_i = -\begin{vmatrix} 1 & x_j & y_j \\ 1 & x_m & y_m \\ 1 & x_p & y_p \end{vmatrix}$$

$$V_e = \frac{1}{6}\begin{vmatrix} 1 & x_i & y_i & z_i \\ 1 & x_j & y_j & z_j \\ 1 & x_m & y_m & z_m \\ 1 & x_p & y_p & z_p \end{vmatrix}$$

V_e is the volume element which may be either positive or negative according to nodal numeration. Index permutation produces N_j, N_m, and N_p. We have

$$Q_{g,e} = -\int_{V_e} N^{\mathrm{T}} \nabla N_1 \, \mathrm{d}V = -\frac{1}{24}\begin{bmatrix} b_i & b_j & b_m & b_p \\ c_i & c_j & c_m & c_p \\ d_i & d_j & d_m & d_p \\ b_i & b_j & b_m & b_p \\ c_i & c_j & c_m & c_p \\ d_i & d_j & d_m & d_p \\ b_i & b_j & b_m & b_p \\ c_i & c_j & c_m & c_p \\ d_i & d_j & d_m & d_p \\ b_i & b_j & b_m & b_p \\ c_i & c_j & c_m & c_p \\ d_i & d_j & d_m & d_p \end{bmatrix}$$

$$Q_{t,e} = \int_{V_e} B^{\mathrm{T}} \mathbf{i} N_1 \, \mathrm{d}V = \frac{1}{24} \begin{bmatrix} b_i & b_i & b_i & b_i \\ c_i & c_i & c_i & c_i \\ d_i & d_i & d_i & d_i \\ b_j & b_j & b_j & b_j \\ c_j & c_j & c_j & c_j \\ d_j & d_j & d_j & d_j \\ b_m & b_m & b_m & b_m \\ c_m & c_m & c_m & c_m \\ d_m & d_m & d_m & d_m \\ b_p & b_p & b_p & b_p \\ c_p & c_p & c_p & c_p \\ d_p & d_p & d_p & d_p \end{bmatrix}$$

The same final comment as in Section 3.1 holds for tetrahedral FE meshes.

3.3. Annular elements with a triangular cross-section

We use a cylindrical reference frame with the z-axis coinciding with the symmetry axis. In Equations (8) and (9) the elementary volume $\mathrm{d}V$ is expressed as

$$\mathrm{d}V = 2\pi r \, \mathrm{d}r \, \mathrm{d}z$$

where r is the radial co-ordinate. Over element e the following approximation is used:

$$\mathrm{d}V = 2\pi r_e \, \mathrm{d}r \, \mathrm{d}z$$

where $r_e = (r_i + r_j + r_m)/3$ is the radial distance of the triangle gravity centre from the z-axis. Using r_e the local stiffness matrix becomes

$$K_e = 2\pi \int_{\Delta_e} \bar{B}^{\mathrm{T}} D \bar{B} r_e \, \mathrm{d}\Delta$$

where $\bar{B}$ is the strain matrix calculated at $r = r_e$. The local coupling matrices take on the following form:

$$Q_{g,e} = -2\pi r_e \int_{\Delta_e} N^{\mathrm{T}} \nabla N_1 \, \mathrm{d}\Delta = -\frac{\pi r_e}{3} \begin{bmatrix} b_i & b_j & b_m \\ c_i & c_j & c_m \\ b_i & b_j & b_m \\ c_i & c_j & c_m \\ b_i & b_j & b_m \\ c_i & c_j & c_m \end{bmatrix}$$

$$Q_{t,e} = 2\pi r_e \int_{\Delta_e} B^{\mathrm{T}}\mathbf{i}N_1 \,\mathrm{d}\Delta = \frac{\pi r_e}{3}\begin{bmatrix} b_i + \dfrac{\Delta_e}{r_e} & b_i + \dfrac{\Delta_e}{2r_e} & b_i + \dfrac{\Delta_e}{2r_e} \\ c_i & c_i & c_i \\ b_j + \dfrac{\Delta_e}{2r_e} & b_j + \dfrac{\Delta_e}{r_e} & b_j + \dfrac{\Delta_e}{2r_e} \\ c_j & c_j & c_j \\ b_m + \dfrac{\Delta_e}{2r_e} & b_m + \dfrac{\Delta_e}{2r_e} & b_m + \dfrac{\Delta_e}{r_e} \\ c_m & c_m & c_m \end{bmatrix}$$

While in the pressure gradient approach the local coupling matrices $Q_{g,e}$ for the two- and the three-dimensional axisymmetric problems differ for the simple multiplying factor $2\pi r_e$, in the total stress approach in addition to $2\pi r_e$ the matrices are also different. This suggests that land subsidence obtained with the FE axisymmetric implementation of the pore pressure gradient and the total stress formulations may not be equal, as will be shown in the next section.

4. INTERESTING NUMERICAL RESULTS

4.1. Average element-wise radius in three-dimensional axisymmetric FE meshes

Consider the simple cylindrical porous medium whose cross-section is displayed in Figure 1. The shadowed area represents the trace of the reservoir. The case of a uniform pore pressure and that of a pressure which varies linearly with r and z are simulated. Since we are concerned with linear poro-elasticity for the purpose of the present analysis the medium Young modulus E can be taken arbitrarily. The results that follow are obtained with $E = 5000\,\mathrm{kg/cm^2}$ and the Poisson ratio $v = 0.25$. Figure 2 shows the land subsidence, i.e. the vertical displacement of the top surface of the porous body of Figure 1, obtained from both formulations discussed in Section 3.3 using the average element-wise radius. It may be noted from Figure 2 that the vertical displacement is the same except in a small region close to the symmetry axis where the pore pressure gradient approach provides a larger value. This is due to the centroid radius approximation as can be seen by performing the volume integration in the calculation of $Q_{g,e}$ and $Q_{t,e}$ with the exact expression for radius r:

$$r = N_i r_i + N_j r_j + N_m r_m$$

The local coupling matrices thus become

$$Q_{g,e} = -2\pi \int_{\Delta_e} N^{\mathrm{T}}\nabla N_1 (N_i r_i + N_j r_j + N_m r_m)\,\mathrm{d}\Delta$$

$$Q_{t,e} = 2\pi \int_{\Delta_e} B^{\mathrm{T}}\mathbf{i}N_1 (N_i r_i + N_j r_j + N_m r_m)\,\mathrm{d}\Delta$$

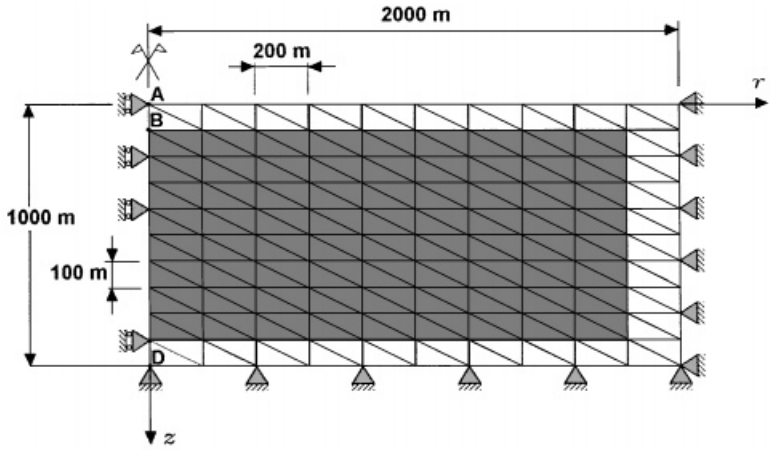

Figure 1. FE grid used to solve the axisymmetric problem. The radial spacing Δr is equal to 200 m.

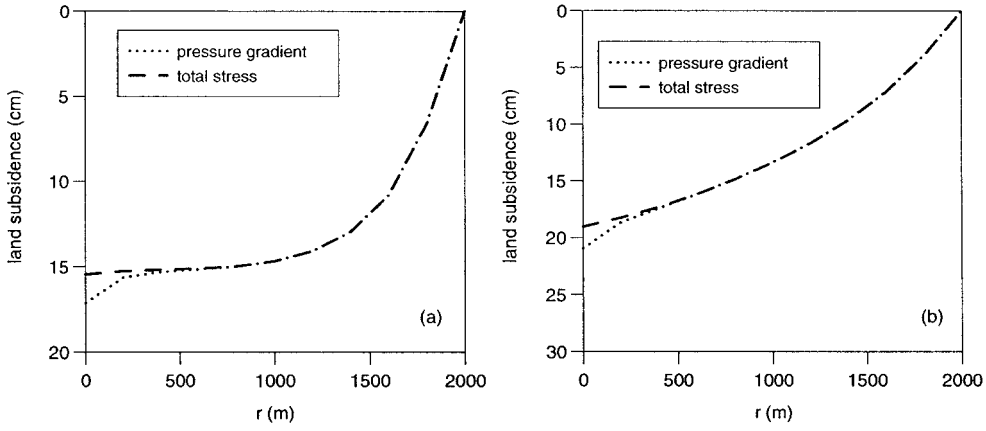

Figure 2. Land subsidence obtained from the axisymmetric FE grid shown in Figure 1: uniform pore pressure $p = 1$ kg/cm^2 within the reservoir (a); linear variation of p (between 1 and 2 kg/cm^2) with r and z within the reservoir (b).

Carrying out the above integrals, and keeping in mind that r also appears in the expression of B, leads to a more accurate result for $Q_{g,e}\mathbf{p}_e$ and $Q_{t,e}\mathbf{p}_e$, i.e. for the local nodal forces $\mathbf{f}_{g,e}$ and $\mathbf{f}_{t,e}$:

$$\mathbf{f}_{g,e} = Q_{g,e}\mathbf{p}_e = -\frac{\pi}{12}\begin{bmatrix} (2r_i + r_j + r_m)(b_i p_i + b_j p_j + b_m p_m) \\ (2r_i + r_j + r_m)(c_i p_i + c_j p_j + c_m p_m) \\ (r_i + 2r_j + r_m)(b_i p_i + b_j p_j + b_m p_m) \\ (r_i + 2r_j + r_m)(c_i p_i + c_j p_j + c_m p_m) \\ (r_i + r_j + 2r_m)(b_i p_i + b_j p_j + b_m p_m) \\ (r_i + r_j + 2r_m)(c_i p_i + c_j p_j + c_m p_m) \end{bmatrix} \tag{10}$$

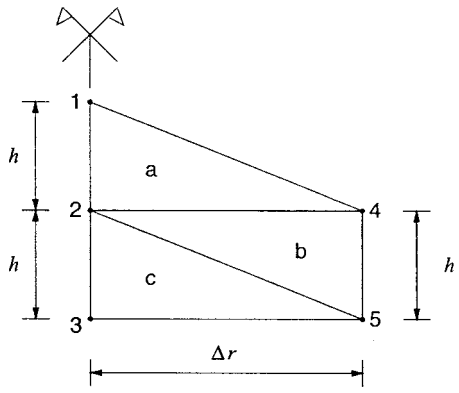

Figure 3. Patch of triangular FE close to the symmetry axis in a three-dimensional axisymmetric problem.

$$\mathbf{f}_{t,e} = Q_{t,e}\mathbf{p}_e = \frac{\pi}{12}\cdot \tag{11}$$

$$\begin{bmatrix} (2r_i + r_j + r_m)b_i p_i + (r_i + 2r_j + r_m)b_i p_j + (r_i + r_j + 2r_m)b_i p_m + 4\Delta_e\left(p_i + \dfrac{p_j}{2} + \dfrac{p_m}{2}\right) \\ (2r_i + r_j + r_m)c_i p_i + (r_i + 2r_j + r_m)c_i p_j + (r_i + r_j + 2r_m)c_i p_m \\ (2r_i + r_j + r_m)b_j p_i + (r_i + 2r_j + r_m)b_j p_j + (r_i + r_j + 2r_m)b_j p_m + 4\Delta_e\left(\dfrac{p_i}{2} + p_j + \dfrac{p_m}{2}\right) \\ (2r_i + r_j + r_m)c_j p_i + (r_i + 2r_j + r_m)c_j p_j + (r_i + r_j + 2r_m)c_j p_m \\ (2r_i + r_j + r_m)b_m p_i + (r_i + 2r_j + r_m)b_m p_j + (r_i + r_j + 2r_m)b_m p_m + 4\Delta_e\left(\dfrac{p_i}{2} + \dfrac{p_j}{2} + p_m\right) \\ (2r_i + r_j + r_m)c_m p_i + (r_i + 2r_j + r_m)c_m p_j + (r_i + r_j + 2r_m)c_m p_m \end{bmatrix}$$

A direct comparison of the assembled loads obtained with the above vectors and those arising from the approximate radius is tedious to make for arbitrary triangles. However, to gain an insight into the role the radius approximation plays the simple mesh of Figure 3 suffices. Assume that nodes 1, 2, and 3 lie on the symmetry axis and compute the force acting on node 2 by assembling the contributions from triangles a, b, and c of Figure 3. Using the aforementioned equations for b_i, b_j, b_m and c_i, c_j, c_m a few calculations with Equations (10) and (11) yield for node 2 the following 'exact' z force component (the r component is of no interest since at $r = 0$ the boundary condition $u_r = 0$ applies):

$$f_{z,\mathrm{ex}}^{(2)} = \frac{\pi(\Delta r)^2}{12}(-p_1 + p_3 - 2p_4 + 2p_5) \tag{12}$$

Note that relationship (12) arises from both Equations (10) and (11). If a similar calculation is made using the average radius approximation a different result according to either formulation

is obtained:

$$f_{z,\mathrm{app}}^{(2)} = \frac{\pi(\Delta r)^2}{9}(-p_1 + p_3 - 2p_4 + 2p_5) \tag{13}$$

(pore pressure gradient formulation)

$$f_{z,\mathrm{app}}^{(2)} = \frac{\pi(\Delta r)^2}{9}(-p_1 + p_3) + \frac{\pi(\Delta r)^2}{18}(-2p_4 + 2p_5) \tag{14}$$

(total stress formulation)

Indeed Equations (13) and (14) are not the same and are both different from Equation (12). Hence r_e exerts a different influence on the two formulations. In particular comparing Equation (12) with Equation (13) we observe that in the pore pressure gradient approach the following relation holds:

$$f_{z,\mathrm{app}}^{(2)} = \tfrac{4}{3} f_{z,\mathrm{ex}}^{(2)}$$

In other words the equivalent nodal load applied on the symmetry axis nodes is 33 per cent larger than the correct one, so a larger subsidence rate at $r = 0$ might be expected from this approach (Figure 4). For the total stress approach we have instead:

$$f_{z,\mathrm{app}}^{(2)} = \tfrac{4}{3} f_{z,\mathrm{ex}}^{(2a)} + \tfrac{2}{3} f_{z,\mathrm{ex}}^{(2b)}$$

where $f_{z,\mathrm{ex}}^{(2a)} = (\pi(\Delta r)^2/12)(-p_1 + p_3)$ and $f_{z,\mathrm{ex}}^{(2b)} = (\pi(\Delta r)^2/12)(-2p_4 + 2p_5)$. The above equations show that $f_{z,\mathrm{app}}^{(2)}$ from the total stress formulation consists of two parts, one which overestimates and one which underestimates the corresponding part of Equation (12) with the associate error usually counterbalanced in a realistic field situation. As a major consequence the prediction of land subsidence over the symmetry axis may result in a much greater accuracy (Figure 4). Let us expand on the previous example a little bit more by assuming a uniform pore pressure p in the reservoir. Then in Figure 3 $p_1 = p_2 = p_3 = p_4 = p_5 = p$ and the vertical force component vanishes on all reservoir axis nodes except on boundary nodes B, C and adjacent nodes A, D of Figure 1. On node A we obtain from Equation (14):

$$f_{z,\mathrm{app}}^{(\mathsf{A})} = \frac{2\pi(\Delta r)^2}{9} p$$

while Equation (12) gives

$$f_{z,\mathrm{ex}}^{(\mathsf{A})} = \frac{\pi(\Delta r)^2}{4} p$$

Hence

$$f_{z,\mathrm{app}}^{(\mathsf{A})} = \tfrac{8}{9} f_{z,\mathrm{ex}}^{(\mathsf{A})}$$

By a similar calculation we get on node B:

$$f_{z,\mathrm{app}}^{(\mathsf{B})} = \frac{\pi(\Delta r)^2}{9} p$$

$$f_{z,\mathrm{ex}}^{(\mathsf{B})} = \frac{\pi(\Delta r)^2}{12} p$$

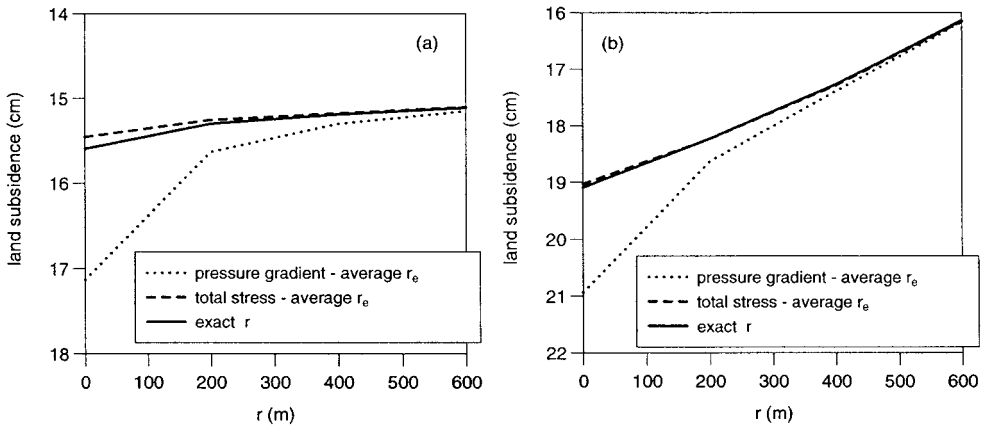

Figure 4. Land subsidence close to the symmetry axis obtained from the FE grid of Figure 1 using the pore pressure gradient and the total stress formulations and the average and correct element radii: uniform $p = 1$ kg/cm^2 (a); linearly variable p between 1 and 2 kg/cm^2 (b).

namely:

$$f_{z,\mathrm{app}}^{(\mathrm{B})} = \tfrac{4}{3} f_{z,\mathrm{ex}}^{(\mathrm{B})}$$

The same findings hold for nodes C and D. Therefore with the total stress formulation and a uniform pressure distribution within the field the vertical forces acting on the axis nodes are partly overestimated and partly underestimated. On the whole they balance to some extent, and this accounts for the superior prediction of land subsidence obtained with this approach and shown in Figure 4(a) which also gives the outcome from the more correct calculation making use of the exact radius in each element. A similar conclusion holds for the example where p varies linearly with r and z (Figure 4(b)).

Equations (12)–(14) point out that the nodal forces on the symmetry axis depend on the square of the first radial spacing Δr with the difference becoming smaller when Δr decreases. This suggests that the formulations using the average and the exact radius expression converge to the same result for $\Delta r \to 0$, as expected on the other hand from the general FE theory. Figure 5 provides the difference between the vertical displacement at $r = 0$ and $z = 0$ (Figure 1) obtained from using Equations (13) and (14) versus Δr. The difference approaches zero as $\Delta r \to 0$. Hence on refined grids the outcomes from both formulations using the average element-wise radius are close and practically coincide with that obtained from performing the integration with the exact radius.

4.2. Influence of boundary integrals

The influence of Neumann boundary integrals in the pressure gradient (8) and total stress (9) formulations is investigated here on a cylindrical porous medium having an internal cavity that represents a pumping well. In Figure 8(a) the well wall of finite radius $R = 0.2$ m is assumed to be a free moving boundary while on the bottom of the cylinder a zero displacement is prescribed. In the reservoir the pore pressure p is set to 1 kg/cm^2 and zero elsewhere. The Poisson ratio is taken

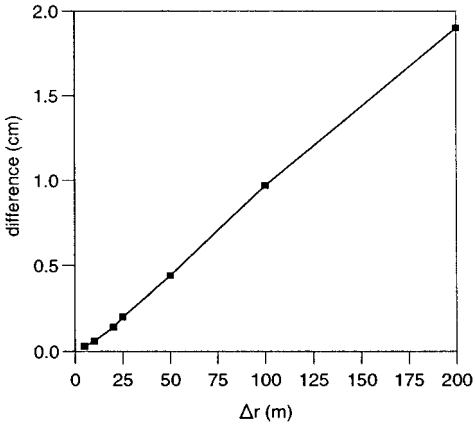

Figure 5. Difference between land subsidence predicted with the pore pressure gradient and the total stress formulations versus the first radial spacing using the average element-wise radius (sample problem of Figure 1).

equal to 0.25 while the Young modulus is that of the sedimentary Northern Adriatic basin and increases with depth [10, Figure 3].

On the inner Neumann boundary we assume a zero variation of the total stress, i.e. $\mathbf{t} = \mathbf{n}p$, thus the elemental boundary force $\tilde{\mathbf{f}}_{t,e}$ in Equations (8) and (9) reads

$$\tilde{\mathbf{f}}_{t,e} = \int_{\Sigma_e} N^{\mathrm{T}} \mathbf{t}_e \, \mathrm{d}\Sigma = \int_{\Gamma_e} N^{\mathrm{T}} \mathbf{n} p 2\pi r \, \mathrm{d}\Gamma = -\tilde{\mathbf{f}}_{p,e} \tag{15}$$

On a well wall node Equation (15) gives $\tilde{f}_{t,e} = 2\pi R p \Delta z_e/2$, with Δz_e the vertical spacing of element e. Note that $\tilde{f}_{t,e} \to 0$ when R approaches 0.

The total stress formulation (9) simply provides

$$K_e \boldsymbol{\delta}_e = Q_{t,e} \mathbf{p}_e$$

While the total stress formulation does not require a boundary integral contribution, in the pore pressure gradient formulation the boundary integral (15) does not vanish and the pore pressure p acts as a distributed force on the well wall.

Figures 6(a) and 6(b) compare the radial and vertical displacements of the well wall for the porous medium of Figure 8(a), respectively, and shows the importance of the boundary integral (15) in the pore pressure gradient approach. Notice that neglecting term (15) has practically no influence on the vertical motion of the well (Figure 6(b)), while it provides a radial displacement with a wrong sign on the wall connected to the reservoir, namely on the pumped portion of the wellbore (Figure 6(a)).

4.3. Infinite pore pressure gradient

Frequently the reservoir is represented as a finite cylindrical volume embedded in a semi-infinite porous medium and subjected to a uniform pore pressure p with an abrupt drop to zero on its

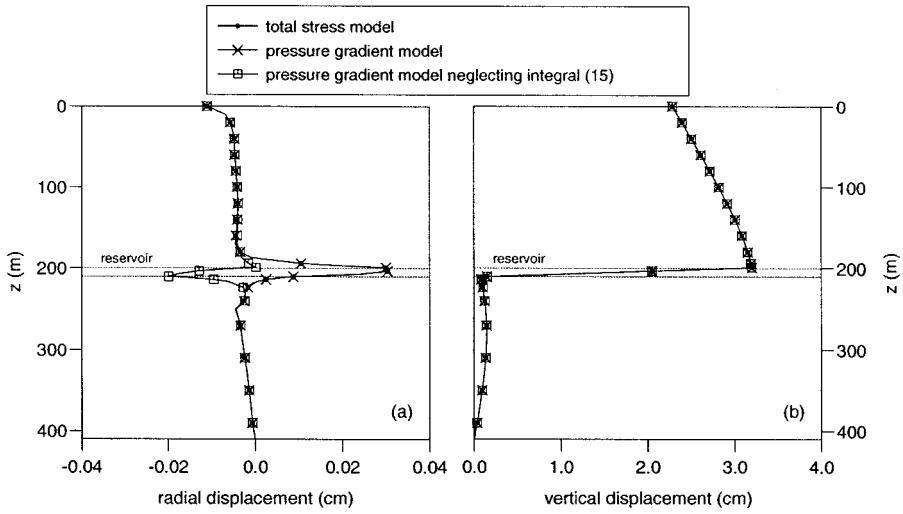

Figure 6. Radial (a) and vertical (b) displacement at $r = R$ as predicted by the two formulations for the porous medium shown in Figure 8(a) with $R = 0.2$ m.

boundary. Analytical solutions of land subsidence for this idealized configuration in a homogeneous medium were developed in References [1, 18, 19] using the concept of nucleus of strain [20] that was derived by analogy from thermoelasticity [21, pp. 66–74]. By distinction, the FE method with the nodal forces as derived in Section 3 for various dimensional settings does not allow to address the exact solution to this problem which is characterized by an infinite pore pressure gradient on the field boundary. Approximate FE solutions may be obtained instead by employing a string of elements around the reservoir across which p goes linearly to zero. The smaller these elements are, the closer the FE solution is to the idealized one.

We discuss in the sequel a modification of the FE equations given in Section 3 for the nodal forces $Q_{g,e}\mathbf{p}_e$ and $Q_{t,e}\mathbf{p}_e$ which allows for an exact FE solution to the infinite pore pressure gradient problem. This solution does not require a set of tiny elements around the gas/oil field where the pore pressure is assumed to dissipate. Since the *ad hoc* modifications are different according to formulation, these are addressed separately.

4.3.1. Pore pressure gradient implementation. For the sake of simplicity let us consider the two-dimensional FE mesh of Figure 7. Using the equations developed in Section 3.1 the global nodal forces on the typical boundary node 2 contributed by triangles a, b, and c under the assumption of a uniform pore pressure p within the reservoir are

$$\text{triangle a:} \quad \begin{cases} f^{(2)}_{\mathsf{a},x} = -\dfrac{1}{6}(b_1 p_1 + b_2 p_2) = -\dfrac{\Delta y}{6}(p_2 - p_1) = 0 \\ f^{(2)}_{\mathsf{a},y} = -\dfrac{1}{6}(c_1 p_1 + c_2 p_2) = \dfrac{\Delta x}{6} p \end{cases}$$

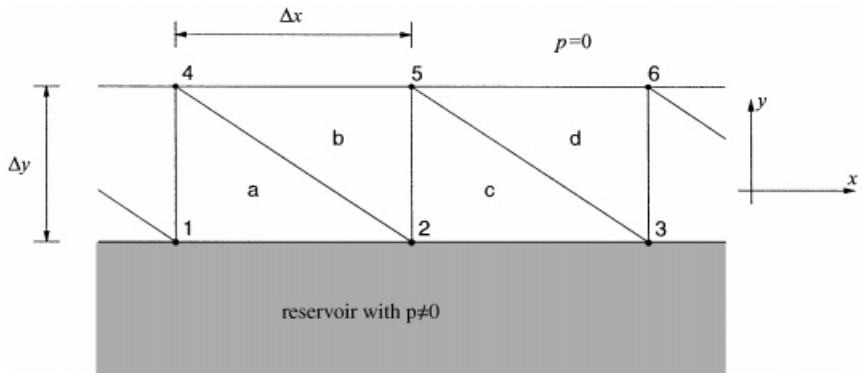

Figure 7. Detail of a two-dimensional FE mesh showing reservoir boundary nodes 1, 2, and 3 and the string of adjacent elements where p naturally dissipates.

$$\text{triangle b:} \quad \begin{cases} f^{(2)}_{\mathrm{b},x} = -\dfrac{1}{6} b_2 p_2 = 0 \\ f^{(2)}_{\mathrm{b},y} = -\dfrac{1}{6} c_2 p_2 = \dfrac{\Delta x}{6} p \end{cases}$$

$$\text{triangle c:} \quad \begin{cases} f^{(2)}_{\mathrm{c},x} = -\dfrac{1}{6}(b_2 p_2 + b_3 p_3) = -\dfrac{\Delta y}{6}(p_3 - p_2) = 0 \\ f^{(2)}_{\mathrm{c},y} = -\dfrac{1}{6}(c_2 p_2 + c_3 p_3) = \dfrac{\Delta x}{6} p \end{cases}$$

Assembling the above contributions yields on node 2:

$$f^{(2)}_{\mathrm{x}} = 0, \qquad f^{(2)}_{\mathrm{y}} = \frac{\Delta x}{2} p \tag{16}$$

Similarly on node 5 opposite to node 2 we obtain from simple calculations:

$$f^{(5)}_{\mathrm{x}} = 0, \qquad f^{(5)}_{\mathrm{y}} = \frac{\Delta x}{2} p \tag{17}$$

Equations (16) and (17) show that the horizontal force component is zero on the horizontal field boundary of Figure 7, while the vertical components are effective on both the reservoir boundary nodes and the opposite external nodes, and do depend only on the horizontal spacing Δx. Hence, shortening the vertical spacing Δy does not affect the force components due to the pore pressure gradient on nodes 2 and 5. In the limiting case when $\Delta y \to 0$ node 5 collapses over node 2 with its contribution to the vertical force component simply added to $f^{(2)}_{\mathrm{y}}$ to provide the overall force $\Delta x p$.

With a similar line of reasoning it can be shown that on the outer reservoir boundary parallel to the y-axis the force component along y is zero and the one along x is independent of Δx, and

again the first string of elements outside the field can be eliminated and the x-component of the force on the vertical boundary nodes set equal twice its value, i.e. Δyp. It is therefore concluded that the infinite pressure gradient problem may be correctly addressed by the FE method by doubling the force components which naturally arise on the reservoir boundary nodes in the standard FE procedure and keeping unloaded the nodes which surround the field. The results obtained above for triangular FE is readily extended to tetrahedral FE.

4.3.2. Total stress implementation. We distinguish between triangular and tetrahedral elements on one side and annular elements with triangular cross-section on the other.

Triangular and tetrahedral FE: Since the development is the same for both FE types we provide the details only for triangles. The extension to tetrahedrons is straightforward. With reference to $Q_{t,e}$ in Section 3.1 the contributions to the nodal forces from triangle e are

$$Q_{t,e}\mathbf{p}_e = \mathbf{f}_{t,e} = \frac{1}{6}\begin{bmatrix} b_i(p_i + p_j + p_m) \\ c_i(p_i + p_j + p_m) \\ b_j(p_i + p_j + p_m) \\ c_j(p_i + p_j + p_m) \\ b_m(p_i + p_j + p_m) \\ c_m(p_i + p_j + p_m) \end{bmatrix} = \frac{\bar{p}_e}{2}\begin{bmatrix} b_i \\ c_i \\ b_j \\ c_j \\ b_m \\ c_m \end{bmatrix} \tag{18}$$

where $\bar{p}_e = \frac{1}{3}(p_i + p_j + p_m)$ is the average pore pressure over triangle e. Equation (18) shows that $\mathbf{f}_{t,e}$ can be obtained from the product between b_i, c_i b_j, etc., and the average element pore pressure $\bar{p}_e$. If an average pore pressure is defined only for the elements within the reservoir while $\bar{p}_e$ is taken to be zero over all elements outside the field, the FE solution is correctly implemented for the problem with an infinite pore pressure gradient on the reservoir boundary. This may be shown using again the example of Figure 7. Assembling the nodal forces contributed only by triangles a, b, c, and d yields

$$f_{\mathsf{x}}^{(2)} = 0, \qquad f_{\mathsf{y}}^{(2)} = -\frac{\Delta x}{2}p$$

on node 2 and

$$f_{\mathsf{x}}^{(5)} = 0, \qquad f_{\mathsf{y}}^{(5)} = \frac{\Delta x}{2}p$$

on node 5. The previous equations state that the horizontal loads arising from these triangles are again zero while the vertical loads acting on a reservoir boundary node and on the external adjacent node are equal and opposite in sign. In the limiting case when $\Delta y \to 0$ these vertical force components cancel. The above outcome may be simply obtained from the FE method implemented in the form of Equation (18) by prescribing an average $\bar{p}_e = 0$ over triangles a, b, c, and d.

Annular FE with triangular cross-section: With reference to $Q_{t,e}$ in Section 3.3, the local nodal forces for element e now read

$$\mathbf{f}_{t,e} = \frac{\pi r_e}{3}\begin{bmatrix} b_i(p_i+p_j+p_m) + \dfrac{\Delta_e}{r_e}\left(p_i + \dfrac{p_j}{2} + \dfrac{p_m}{2}\right) \\ c_i(p_i+p_j+p_m) \\ b_j(p_i+p_j+p_m) + \dfrac{\Delta_e}{r_e}\left(\dfrac{p_i}{2} + p_j + \dfrac{p_m}{2}\right) \\ c_j(p_i+p_j+p_m) \\ b_m(p_i+p_j+p_m) + \dfrac{\Delta_e}{r_e}\left(\dfrac{p_i}{2} + \dfrac{p_j}{2} + p_m\right) \\ c_m(p_i+p_j+p_m) \end{bmatrix}$$

which can be rewritten as

$$\mathbf{f}_{t,e} = \pi r_e \bar{p}_e \begin{bmatrix} b_i \\ c_i \\ b_j \\ c_j \\ b_m \\ c_m \end{bmatrix} + \pi \Delta_e \begin{bmatrix} \frac{1}{3}[p_i + 0.5(p_j+p_m)] \\ 0 \\ \frac{1}{3}[0.5p_i + p_j + 0.5p_m] \\ 0 \\ \frac{1}{3}[0.5(p_i+p_j) + p_m] \\ 0 \end{bmatrix} \tag{19}$$

with $\bar{p}_e = \frac{1}{3}(p_i + p_j + p_m)$ again the average element pore pressure. In Equation (19) it is approximately true that

$$\tfrac{1}{3}[p_i + 0.5(p_j+p_m)] \cong \tfrac{1}{3}[0.5p_i + p_j + 0.5p_m] \cong \tfrac{1}{3}[0.5(p_i+p_j) + p_m] \cong \tfrac{2}{3}\bar{p}_e$$

Hence, Equation (19) becomes

$$\mathbf{f}_{t,e} = \pi r_e \bar{p}_e \begin{bmatrix} b_i + \dfrac{2}{3}\dfrac{\Delta_e}{r_e} \\ c_i \\ b_j + \dfrac{2}{3}\dfrac{\Delta_e}{r_e} \\ c_j \\ b_m + \dfrac{2}{3}\dfrac{\Delta_e}{r_e} \\ c_m \end{bmatrix} \tag{20}$$

Again if $\bar{p}_e = 0$ is taken over all elements outside the reservoir we obtain the correct FE solution to the three-dimensional axisymmetric problem (e.g. a cylindrical field) where the pore pressure goes abruptly to zero on the reservoir boundary.

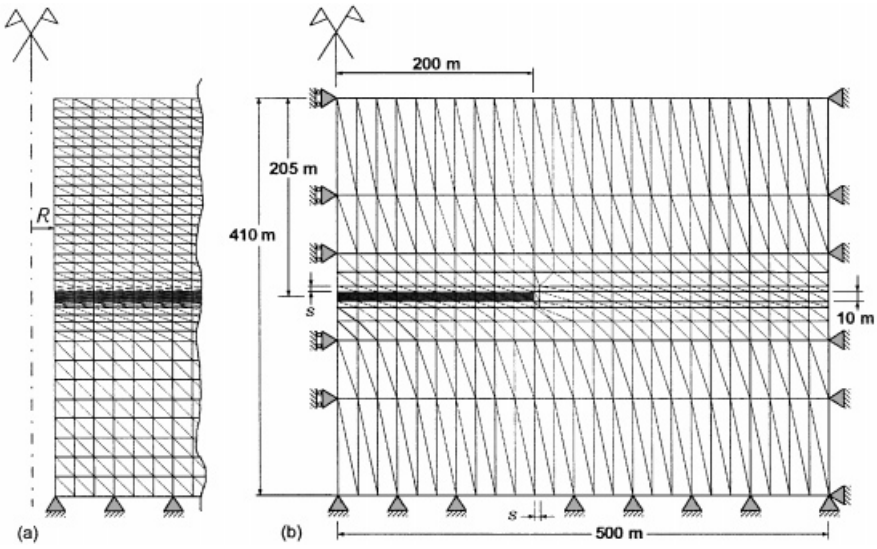

Figure 8. Three-dimensional axisymmetric FE grids embedding a disk-shaped reservoir with a different refinement. The finer grid (a) is used to evaluate the influence of the boundary integrals in displacement calculations at the well wall with radius $R = 0.2$ m. The coarser grid (b) is used to validate the implementation of the infinite pore pressure gradient model. The shadowed area represents the reservoir, i.e. the area over which the strength source is distributed.

4.3.3. Numerical solution to the infinite pore pressure gradient problem. In this section it is shown that the special FE solution developed previously for an infinite pore pressure gradient on the reservoir boundary is the limiting case of the standard FE solution where the string of elements adjacent to the field across which pore pressure dissipates linearly is made infinitely thin. The numerical experiments are performed with a cylindrical reservoir embedded in a porous medium discretized by the annular triangulation of Figure 8(b). The pore pressure p within the reservoir is uniformly distributed and equal to 1 kg/cm^2 with the elastic constants the same as those used in Section 4.2. Out-side the reservoir a zero pressure is assumed everywhere. However, in the standard FE implementation the elements close to the field are a partial source of strength as well.

We denote by s the thickness of the elements which surround the reservoir (Figure 8). Figure 9 shows the land subsidence as obtained from the standard FE method described in Section 3.3 and the FE method modified in Sections 4.3.1 and 4.3.2 to account for the infinite pore pressure gradient on the field boundary. As can be seen from Figure 9 land subsidence from the traditional FE method is quite sensitive to s. However, as s approaches zero the FE solution gradually comes close to the solution obtained from the FE implementation discussed in Section 4.3.1 or 4.3.2. Thus these ad hoc implementations allow to address correctly the problem of an idealized reservoir with a discontinuous pore pressure p on the boundary without the need for introducing a set of elements over which p is assumed to dissipate. Also note in Figure 9 that the solid profile is obtained from both formulations with the approximation of the average element-wise radius on performing the FE integration. On account of the relatively small radial spacing used in this example (equal to 20 m, Figure 8) the two formulations provide practically the same outcome at $r = 0$ as well.

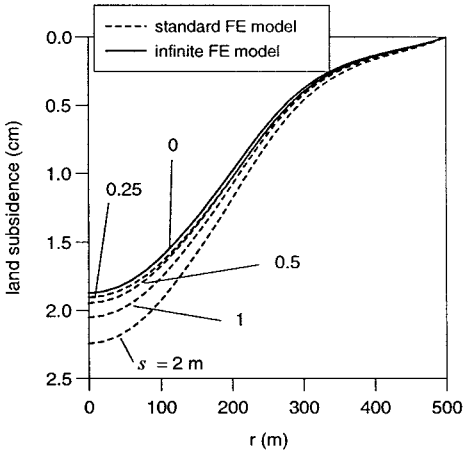

Figure 9. Land subsidence as obtained from the infinite pore pressure gradient FE model using either the pore pressure gradient or the total stress formulation (solid line) and from the standard FE method (dashed lines).

5. CONCLUSIONS

Land subsidence above depleted gas/oil fields can be addressed by the FE method using either the pore pressure gradient formulation or the total stress formulation. Both approaches are equivalent at the global assembled level but generate different local forces at the element level. If three-dimensional axisymmetric problems are solved with the use of the average element-wise radius in the FE integration, the equivalence does not hold at the global level as well, and the two formulations predict a different land subsidence in the vicinity of the symmetry axis. The total stress model provides a more accurate result and an argument is developed to account for the better performance of this approach. At the global level the two formulations may be reconciled by the introduction of appropriate boundary integrals. An example of this has been shown with the reservoir pumped by a well of finite radius. Finally, two modifications to the standard FE method have been discussed which allow for the correct simulation of an infinite pressure gradient, i.e. a discontinuity of the pore pressure on the field boundary. These modified FE implementations avoid the need for introducing a string of tiny elements around the field where the pore pressure variation is assumed to dissipate.

ACKNOWLEDGEMENTS

This study has been partially funded by the Italian MURST project 'Analisi Numerica: Metodi e Software Matematico" and by the Sardinian Regional Authorities.

REFERENCES

1. Geertsma J. Land subsidence above compacting oil and gas reservoirs. *Journal of Petroleum Technology* 1973; **25**:734–744.

2. Gambolati G, Freeze RA. Mathematical simulation of the subsidence of Venice. 1. Theory. *Water Resources Research* 1973; **9**(3):721–733.
3. Lewis RW, Schrefler BA. A fully coupled consolidation model of the subsidence of Venice. *Water Resources Research* 1978; **14**(2):223–230.
4. Zienkiewicz OC, Taylor RL. *The Finite Element Method*, (4th edn), vol. 1. McGraw-Hill: London, 1989.
5. Zienkiewicz OC. *The Finite Element Method in Engineering Geoscience* (4th edn). McGraw-Hill: London, 1991.
6. Zienkiewicz OC. *Introductory Lectures on the Finite Element Method*. CISM Courses and Lectures, vol. 130. Springer: Berlin, 1973.
7. Gambolati G, Ricceri G, Bertoni W, Brighenti G, Vuillermin E. Mathematical simulation of the subsidence of Ravenna. *Water Resources Research* 1991; **27**(11):2899–2918.
8. Gambolati G, Putti M, Teatini P. Coupled and uncoupled poroelastic solutions to land subsidence due to groundwater withdrawal. In *ASCE Engineering Mechanics Conference*, *Mini Symposium on Poroelasticity*, Lin YK, Su TC (eds). ASCE: New York, 1996; 483–486.
9. Gambolati G, Putti M, Teatini P. Land subsidence. In *Hydrology of Disasters*, chapter 9, Singh VP (ed.). Kluwer Academic P.C.: Dordrecht, 1996; 231–268.
10. Gambolati G, Teatini P, Bertoni W. Numerical prediction of land subsidence over Dosso degli Angeli gas field, Ravenna, Italy. In *Land Subsidence—Current Research and Case Studies* (*Proceedings of the Joseph F. Poland Symposium on Land Subsidence*, Sacramento (CA), October 1995), Borchers J (ed.). Star Publ. Co: Belmont, CA, 1998; 229–238.
11. Yeh HD, Lu RH, Yeh GT. Finite element modelling for land displacements due to pumping. *International Journal for Numerical and Analytical Methods in Geomechanics* 1996; **20**:79–99.
12. Lewis RW, Sukirman Y. Finite element modelling for simulating the surface subsidence above a compacting hydrocarbon reservoir. *International Journal for Numerical and Analytical Methods in Geomechanics* 1993; **18**:619–639.
13. Gatmiri B, Delage P. A formulation of fully coupled thermal-hydraulic-mechanical behaviour of saturated porous media—Numerical approach. *International Journal for Numerical and Analytical Methods in Geomechanics* 1997; **21**:199–225.
14. Ghaboussi J, Wilson EL. Flow of compressible fluid in porous elastic media. *International Journal for Numerical Methods in Engineering* 1973; **5**:419–442.
15. Reed MB. An investigation of numerical errors in the analysis of consolidation by finite elements. *International Journal for Numerical and Analytical Methods in Geomechanics* 1984; **8**:243–257.
16. Sloan SW, Abbo AJ. Biot consolidation analysis with automatic time stepping and error control, Part 1: theory and implementation. *International Journal for Numerical and Analytical Methods in Geomechanics* 1999; **23**:467–492.
17. Terzaghi K, Peck RB. *Soil Mechanics in Engineering Practice* (2n edn). Wiley: New York, 1967.
18. Geertsma J. A basic theory of subsidence due to reservoir compaction: the homogenous case. *Verhandelingen van het Koninklijk Nederlands Geologisch Mijnbouwkunding Genootschap* 1973; **28**:43–62.
19. Geertsma J, Van Opstal G. A numerical technique for predicting subsidence above compacting reservoirs, based on the nucleus of strain concept. *Verhandelingen van het Koninklijk Nederlands Geologisch Mijnbouwkunding Genootschap* 1973; **28**:63–78.
20. Geertsma J. Problems of rock mechanics in petroleum production engineering. In *Proceedings of 1st Congress on International Society of Rock Mechanics*, Lisbon, 1966; 585–594.
21. Nowacki W. *Thermoelasticity*. Pergamon Press: Oxford, 1962.

